Structural and electronic properties of lithium intercalated graphite LiC_6

K. R. Kganyago and P. E. Ngoepe*
Materials Modelling Center, School of Physical and Mineral Sciences, University of the North, P/Bag X 1106, Sovenga, 0727, South Africa

(Received 3 April 2003; revised manuscript received 25 June 2003; published 26 November 2003)

We calculate the lattice properties and electronic structure of graphite and LiC_6 within the most widely used density-functional theory implementation, the local density approximation (LDA). Improvements to the LDA in the form of a generalized gradient approximation (GGA) are explored. Structural parameters predicted by the LDA, as expected, underestimate experiment within a 1%–2% margin of accuracy. The GGA does not give a good account in the prediction of lattice parameter *c*, especially in graphite, although it does give a reliable description of LiC_6. The effect on intercalating lithium into graphite, where charge transfer from lithium to carbon layers (graphenes) is expected, is discussed from the valence charge density, partial density of states, and energy band structure plots. The latter plot is also compared with inelastic neutron scattering results and low-energy electron diffraction results. We extend this work by calculating the elastic constants and bulk modulus for both graphite and LiC_6 structures. These results are in excellent agreement with the available experimental data. The calculated hydrostatic pressure dependence of the crystal structures is also found to be in good agreement with the results of high-resolution x-ray structural studies and with other experimental data as well as with other calculations. The analysis of electronic structure at 0 GPa (ambient pressure) is used to resolve inconsistencies between previous LDA calculations.

DOI: 10.1103/PhysRevB.68.205111 PACS number(s): 71.20.−b, 64.30.+t, 71.10.−w, 31.25.−v

I. INTRODUCTION

Graphite intercalation compounds (GIC's) are formed through a process of electron exchange between the host layers and different types of atoms and molecules. Graphite is an interesting example of a layered material with only *s* and *p* ($2s^2$ and $2p^4$) electrons contributing to the valence band. This consists of weak π bonds originating from $2p_z$ orbitals between the layers along the crystallographic *c* axis. Detailed band structure calculations have been made for graphite[1,2] up to energies 50 eV above Fermi energy. The so-called first-stage lithium intercalated graphite LiC_6 is one of the most thoroughly studied alkali-graphite compounds playing an important role in understanding the performance of carbon-based anodes in rechargeable Li-ion batteries.[3] Upon intercalation of Li ions into graphite, some fraction of the Li $2s$ valence electron density becomes delocalized on the carbon layers. On the basis of band structure calculations it is proposed that lithium acts as an electron donor in LiC_6. The previous π^* (antibonding) orbitals in graphite are partially filled by the excess $2s$ electrons from the lithium atoms and the Fermi level is raised accordingly. These generate ionic binding between the layers, hence generating high-mobile-charge carriers in LiC_6. Little is known about the effect of intercalation on the shape of graphite and the diffusivity of the Li ion during the cycling process. In the present paper we focus our attention on the structural aspects and the electronic structure of LiC_6.

A wealth of experimental data has been amassed relating to the equation of state[4–9] (EOS) and elastic constants[8,10–15] of graphite. Measurements of electronic properties of graphite have been extensively carried out using x- ray,[5,9,16] Raman scattering,[8,12,17] synchrotron radiation-induced photoelectron spectroscopy (XPS),[18] infrared reflectance,[8,19] inelastic neutron scattering,[20,21] angle-resolved photoemission,[22–24] and angle-resolved inverse photoemission[24–30] experiments. Energy density curves of soft x-ray emission of graphite and the band densities of states were measured by Dose *et al.*[25] and inverse photoemission spectroscopy was used to detect the interlayer states in graphite.[26] These states were also revealed in the carbon *K* near-edge x-ray absorbed fine structure (NEXAFS) measurement.[16] Considerable work has been performed on the valence-band structure of graphite using x-ray emission experiments.[31,32] Analysis of the direction of polarization of the emitted x rays shows σ and π components of states originating from atomic *p* states.

The elastic and thermal properties of graphite have been extensively studied by x-ray[5,9] and inelastic neutron scattering[20] techniques. Graphite has been examined under high pressure of up to 73 GPa over several decades.[17] *In situ* x-ray diffraction[6] and micro-Raman[17] measurements reveal evidence of a phase transition at 15–20 GPa. Isothermal *c*-axis compressibility and thermal expansion have been measured[33] using neutron diffraction at pressures up to 20 GPa. Most theoretical studies of the compressibility have used phenomenological models of the interatomic forces.[34,35] These models appear to describe the compressional elastic constant C_{33} and its variation with pressure reasonably well to 1 GPa, but are inappropriate for describing the shear modulus C_{44} (Ref. 36) Jansen and Freeman[37] used the all-electron full-potential linearized augmented plane-wave (FLAPW) method to calculated elastic constants $C_{11}+C_{12}$ and C_{33} for graphite with C_{13} different from experiment. Chan *et al.*[38] used both *ab initio* pseudopotentials and linear combination of atomic orbitals (LCAO) to calculate $C_{11}+C_{12}$ for graphite. Al-Jishi and Dresselhaus[39] reported the elastic constant for graphite using the Born–von Karman lattice-dynamical model. Lang *et al.*[40] also used the De Lua-

nay lattice dynamics model to calculate the elastic constants for both graphite and LiC_6.

The band structure of graphite in an energy range close to the Fermi energy was first calculated by McLure[41] and Slonczewski and Weins[42] (commonly known as the SWMcC model). The electronic structure of graphite has been calculated self-consistently by means of the local density approximation (LDA) by numerous workers using different computational methods such as the LCAO,[43] Thomas-Fermi plus gradient approximation,[44] the Korringa-Kohn-Rostoker[45,46] (KKR) method,[47] the FLAPW method,[26,37,48] full potential linear muffin-tin-orbital (FLMTO) method,[49–51] the *ab initio* pseudopotential (PP) method,[52–57] linear muffin-tin-orbital (LMTO) method[49] within the atomic sphere approximation (ASA) and all-electron full-potential linear combination of Gaussian-type orbital fitting-function (LCGTO-FF) technique.[58] The LCGTO-FF technique has been used to calculate the electronic structure, equation of state, and elastic constants of graphite. Electronic structure calculations, to date, have been carried out on the high-pressure behavior[37,59–61] of graphite. Calculations on compressed hexagonal graphite structure have been performed[50] and show that the *c* axis becomes much more compressed than the *a* axis. Recent density-functional theory (DFT) calculation of the quasi-two-dimensional (quasi-2D) electron systems, with graphite as an example, suggested that the generalized gradient approximation (GGA) gives poorer descriptions of 2D systems than the LDA.[62]

The physical properties of LiC_6 have been studied through angle-resolved photoelectron spectroscopy,[22,63] nuclear magnetic resonance (NMR),[64] Raman spectroscopy,[64] specific heat, metallic reflection,[65] anisotropic conductivity,[65] low-energy photoemission spectroscopy,[66] and optical spectra measurements. Charge transfer effects have been investigated experimentally for LiC_6 using angle-resolved photoelectron spectroscopy[22] and x-ray photoemission spectra.[67] The pressure dependence of the experimental ^{7}Li NMR spectra has been reported for LiC_6 at 232 and 293 K (Ref. 68) with the compressibility predicted as $\kappa_c = 1.7 \times 10^{-12}$ cm^2/dyn. Neutron diffraction measurements[33] of the *c*-axis compressibility κ_c at 300 K (for hydrostatic pressures <2.5 GPa) and *c*-axis thermal expansion in the temperature interval 300–700 K were also probed for LiC_6. The compressibility was reported as $\kappa_c = 1.43 \pm 0.02 \times 10^{-12}$ cm^2/dyn for hydrostatic pressure $\leqslant 23$ kbar. The latter results were also reported from neutron and x-ray scattering measurements.[69,70] Several theoretical investigations of the electronic structure for LiC_6, such as PP calculations,[57,71–75] have been carried out. The valence charge density of LiC_6 was evaluated[73] based on earlier band structure calculations by Holzwarth *et al.*[72] using the KKR technique. It was established that the conduction bands of LiC_6 are essentially derived from unoccupied π bands of graphite and the occupied carbon σ bands are found to be relatively unaffected by intercalation.

II. SCOPE OF THE PAPER

Several measurements on structural properties and calculated lattice parameters of graphite have been reported (see Sec. I) at ambient pressure. However, not much work appears on the pressure variation of the relative lattice parameters of graphite and, in particular, LiC_6. There is a considerable less theoretical work on compressed graphite and almost no pressure work reported in literature on LiC_6. Our current work presents the first high-pressure theoretical results of LiC_6. Such calculations are of interest since the variation of the *c* axis with pressure in graphite is an important observable.

In Sec. III, we review the *ab initio* total-energy pseudopotential method, a self-consistent density-functional approach using norm-conserving pseudopotentials and ultrasoft pseudopotentials within both the local density and generalized gradient approximations for exchange and correlation. In Sec. IV we discuss in detail the impact of the LDA and GGA on the prediction of the lattice parameters of graphite and LiC_6. In Sec. V we present results obtained on the structural parameters such as the lattice constants, volume, and bulk moduli. Section VI shows and discusses the elastic constants for both graphite and LiC_6, where both LDA and GGA results are compared with available experimental data. In Sec. VII we discuss partial density of states (PDOS) of graphite and LiC_6. In this work we therefore aim to present the new pressure work on LiC_6 and the calculated elastic constants within both the LDA and GGA. We also aim to improve the understanding of the electronic structure of both graphite and LiC_6, which will be achieved by calculating and comparing the DOS of both systems.

III. METHODOLOGY

All calculations use the total-energy (E^{tot}) code CASTEP,[76] which employs pseudopotentials to describe electron-ion interactions and represents electronic wave functions using a plane-wave basis set.[77] The total energy is calculated both within the framework of the LDA, the Perdew-Zunger[78] parametrization of the numerical results of Ceperley and Alder,[79] for the exchange-correlation energy, and the nonlocal or gradient-corrected approximations [Perdew-Burke-Ernzerhof[80] (PBE)] implemented according to the method described by White and Bird.[81] The PBE form of the GGA is designed to be more robust and accurate than the original [Becke[82] (B) and Perdew-Wang[83] (PW)] GGA formulations which we used in our earlier calculations. The interactions between the ionic cores and the electrons are described by the Troullier-Martins[84] pseudopotential, the pseudopotential in Kleinman-Bylander[85] form, and the associated Vanderbilt[86] pseudopotential. The earlier pseudopotentials were specifically used for the calculations of electronic properties rather than structural parameters, the latter being predicted by ultrasoft pseudopotential[86] (USP) since it requires significantly less computational resources. We also used the USP for high-pressure studies.

In order to describe the relatively hard potentials of carbon and lithium atom, cutoff energies of up to 600 eV for graphite and 900 eV for LiC_6 were used for the expansion of the wave functions. The pseudowave functions, the smooth part of the charge density, and the potential are represented on a fast-Fourier-transform (FFT) grids of $18 \times 18 \times 50$ and

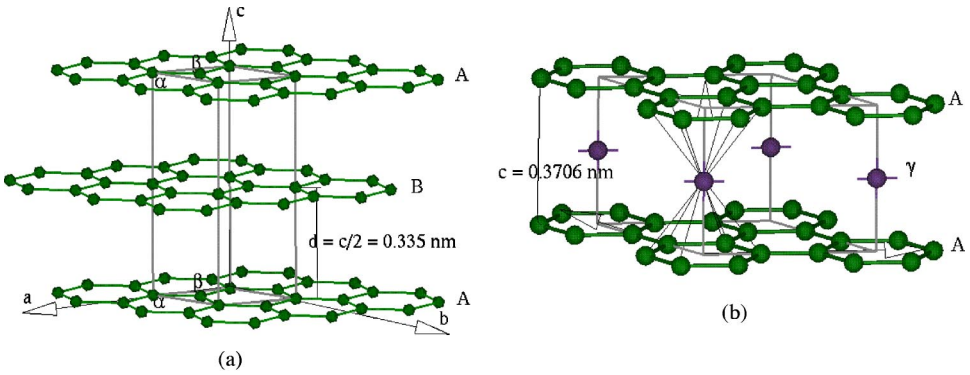

FIG. 1. (a) Schematic drawing of the crystal structure of hexagonal graphite showing the *AB* layer stacking sequence and the unit cell. (b) Structure of Li-intercalated graphite compound LiC_6 (stage 1) with the $A\gamma A$ stacking sequence, γ being the fictitious Li-ion layer midway the graphenes.

$32\times32\times27$ for graphite and LiC_6, respectively. These minimum FFT grids applied to the exchange-correlation potential $[V_{xc}(G-G')]$ are sufficient for the cutoff energies. The 24 and 15 k points were generated with the Monkhorst-Pack[87] scheme with parameters $(9\times9\times4)$ and $(5\times5\times6)$ for graphite and LiC_6, respectively. Each k point in the irreducible Brillouin zone was represented with an equivalent of 3650 and 3200 plane waves. A set of single-point energy calculations was carried out for each structure (graphite and LiC_6) to obtain structural parameters corresponding to minimum energy. We calculated the ground-state total energy over a wide range of volumes (lattice parameter $a=b$, for a constant value of c) and lattice constants a and c.

Another set of calculations was carried out to produce the EOS of graphite and LiC_6 up to 25 GPa. Geometry optimization was performed using a Broyden-Fletcher-Goldfarb-Shanno (BFGS) based minimization technique at a fixed value of applied hydrostatic pressure, which is methodologically similar to the experimental procedure of measuring the EOS.[88] The total energies were corrected using the finite-basis set correction method developed by Francis and Payne.[89] Calculations were considered converged when the residual forces were less than 0.05 eV $Å^{-1}$, the displacement of atoms during the geometry optimization steps were less than 0.001 Å, and the residual bulk stress was less than 0.1 GPa. At every unit cell volume the atomic positions were relaxed under Hellmann-Feynman forces and the unit cell parameters were also optimized to minimize enthalpy. The calculated cell volumes were then used to construct the equation of state, which was fitted to a Murnaghan equation to obtain the bulk modulus B and its pressure derivative B'.

The last set of calculations was performed to obtain the elastic coefficients of graphite and LiC_6. Practical methods for determining the elastic coefficients from first principles usually set either the stress or strain to a finite value, optimize any free parameters of the structure, and calculate the other property (strain or stress, respectively). Applying a given homogeneous deformation (the strain) and calculating the resulting stress requires far less computational effort, since the unit cell is fixed and only the ionic positions require optimization. Two strain patterns—one with nonzero first and fourth components and another with a nonzero third component—give stresses related to all five independent elastic coefficients for the hexagonal system. Two positive and two negative amplitudes were used for each strain component, and then the elastic stiffnesses were determined from a linear fit of the calculated stress as a function of strain. Geometry optimization at zero pressure was performed with the variable lattice parameter and full relaxation of the internal coordinates. Calculations were considered to be converged when the maximum force on an atom was below 0.01 eV $Å^{-1}$ and elastic coefficients are converged to 1 GPa with these settings.

IV. LOCAL DENSITY AND GENERALIZED GRADIENT CORRECTION EFFECT TO THE ELECTRON DENSITY AND EQUATION OF STATE

An interplay between electronic delocalization and contribution to bonding by van der Waals forces is explored from the calculated charge density of *ABABA*-stacked graphite [see Fig. 1(a)]. Figure 2(a) presents the isodensity lines along the c axis: a section is made perpendicular to the graphene sheet. This figure clearly shows the different behavior of in-plane and interplanar bonding, as well as the *ABABA*-stacking graphite. In order to analyze the interlayer interaction, we subtract the isolated-graphite-layer electronic density [Figs. 2(b) and 2(c)] from the graphite electronic density [Fig. 2(a)]. The result [Fig. 2(d)] shows the isolated effects specific to the interplanar interactions. This figure shows that the electronic charge in the neighborhood of the α atoms is depleted along the c-axis direction, in contradiction with the weak covalent picture on the bonding. These electrons are transferred to the neighborhood of the β atoms and also in the interplanar region. This increase in the charge, positioned between the two layers, extends homogeneously in the entire interplanar region. On contrary, in the α-β direction, a small lack of electrons appears near β and a little excess near α. This delocalization of the electrons in the interplanar region was reported by Charlier *et al.*[90] and is used in our study to evaluate the corrections to the exchange-correlation term of the Kohn-Sham equations and understanding of structural changes in the graphite intercalated compound LiC_6.

A comparison of the c lattice parameter predictions by the two forms of exchange correlation—the LDA and GGA—is enlightening. Table I and Fig. 3(a) show that the LDA calculation underestimates this value in graphite. However, both Becke[82] and Perdew-Wang[83] GGA's fail to predict the value of c, as noted from the variation of the total energy with cell parameters in Fig. 3(c). Similar results were recently observed for graphite[91] and graphite intercalated with H_2

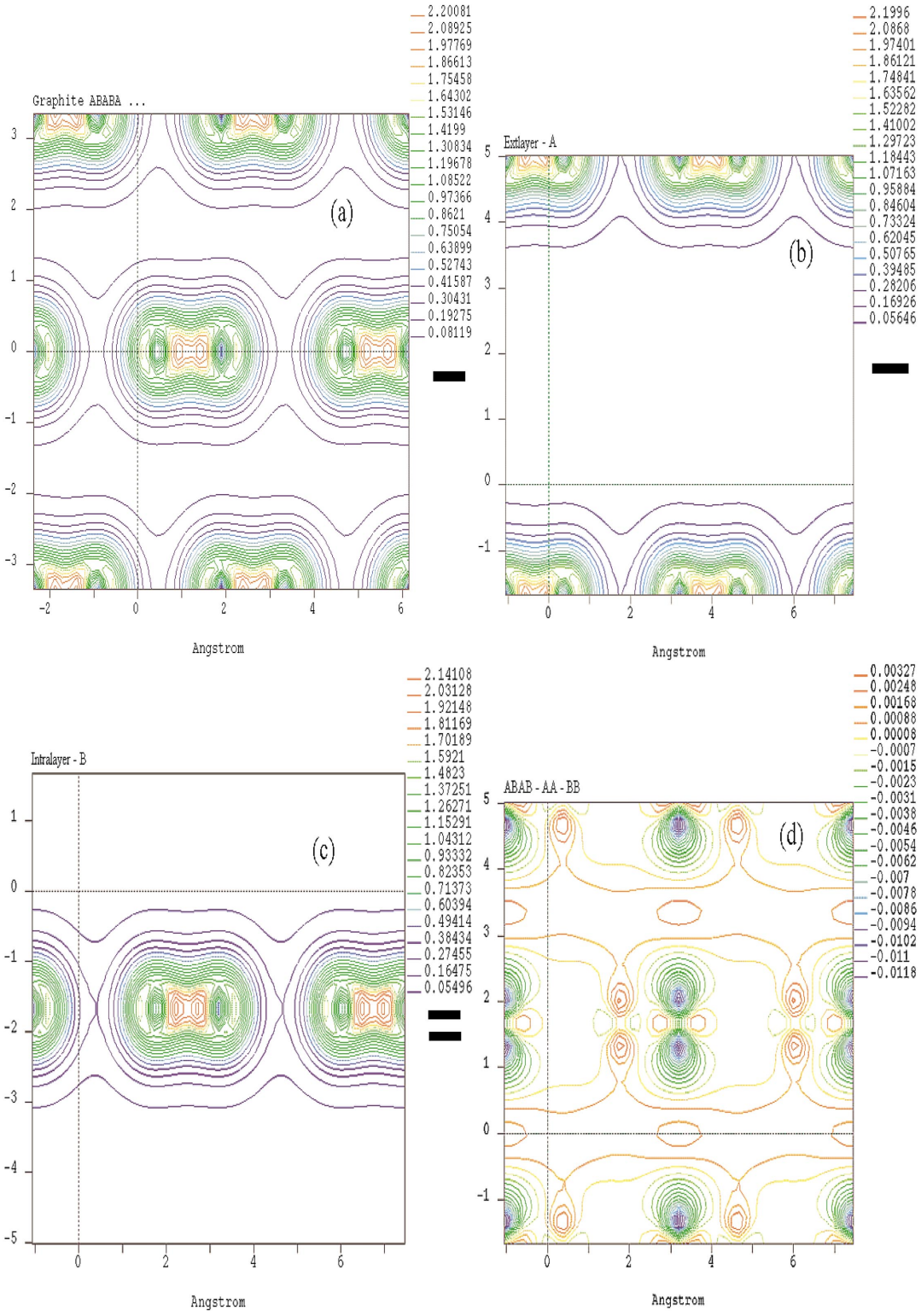

FIG. 2. (Color) *Ab initio* electron pseudocharge density for (a) graphite in a plane perpendicular to the **A** and **B** graphene sheets, (b) **A**-type isolated graphite layer along the *c* axis as in (a), and (c) **B**-type isolated graphite layer along the *c* axis as in (a). The contour plots ranges between 0.05*e*/Å and 2.23*e*/Å. (d) Contour plot of the transfer of charge due to stacking of the graphene layers obtained by the process described in this figure: density of graphite (a) minus that of reference graphite layers: **A** plane (b) and **B** plane (c).

molecules.[92] For LiC_6, predictions of *c* by LDA and GGA calculations are close to experimental values [see Figs. 3(b) and 3(d)]. The intraplanar C-C bond lengths follow similar trends. The LDA and GGA overestimate the *c* parameter by ~8%. Hence it may be concluded that the GGA form of the exchange correlation appears to be inadequate in handling

TABLE I. Calculated and experimental structural parameters of graphite and LiC_6.

		LDA	GGA-PW	Experimental
Graphite	a (Å)	2.450	2.44	2.460[a]
	c (Å)	6.500		6.700[a]
	V (Å^3)	34.175	33.893	35.100[a]
	C-C (Å)	1.415	1.409	1.420[a]
LiC_6	a (Å)	4.300	4.300	4.305[b]
	c (Å)	3.700	3.800	3.706[b]
	V (Å^3)	59.073		59.500[b]
	C-C (Å)	1.430	1.440	1.441[b]

[a]Reference 20.
[b]Reference 71.

the weaker interlayer van der Waals bonds in graphite. It however approximates the interlayer bonding in LiC_6 better, which, though weak, is stronger than in graphite. Indeed, previous studies[74] have shown that lithium ion in LiC_6 contributes charge to a π-density environment and thereby slightly increases interplanar bonding. Hence the GGA, whose contribution is supposed to be short ranged, gives a more reasonable prediction of this bond in LiC_6.

The calculated valence electron pseudocharge density of graphite in the (010) plane perpendicular to the graphenes is given in Figs. 4(a) and 4(b) for the LDA and GGA, respectively. A high concentration of charge is observed between neighboring carbon atoms, suggesting covalent bonding, in agreement with previous LDA results.[55] Generally, charge distributions appear similar for the LDA and GGA on this scale. A contour plot of the difference between the LDA and GGA electron densities on a similar plane is given in Fig. 4(c). The magnitude of difference density, ρLDA$-\rho$GGA, is very small compared with the total electron densities. The regions of positive contour indicate that the LDA density is larger in the graphene ring, hence tending to contract the ring. The GGA density has a slightly higher contribution in the bond connecting neighboring carbon atoms of the graphene ring. The LDA charge density is dominant in the weak π-bonding region between layers with no visible trace of the GGA charge density. Indeed, this explains why the GGA fails to predict the c lattice parameter in structural calculations.

In order to compare the effects of the LDA and GGA on

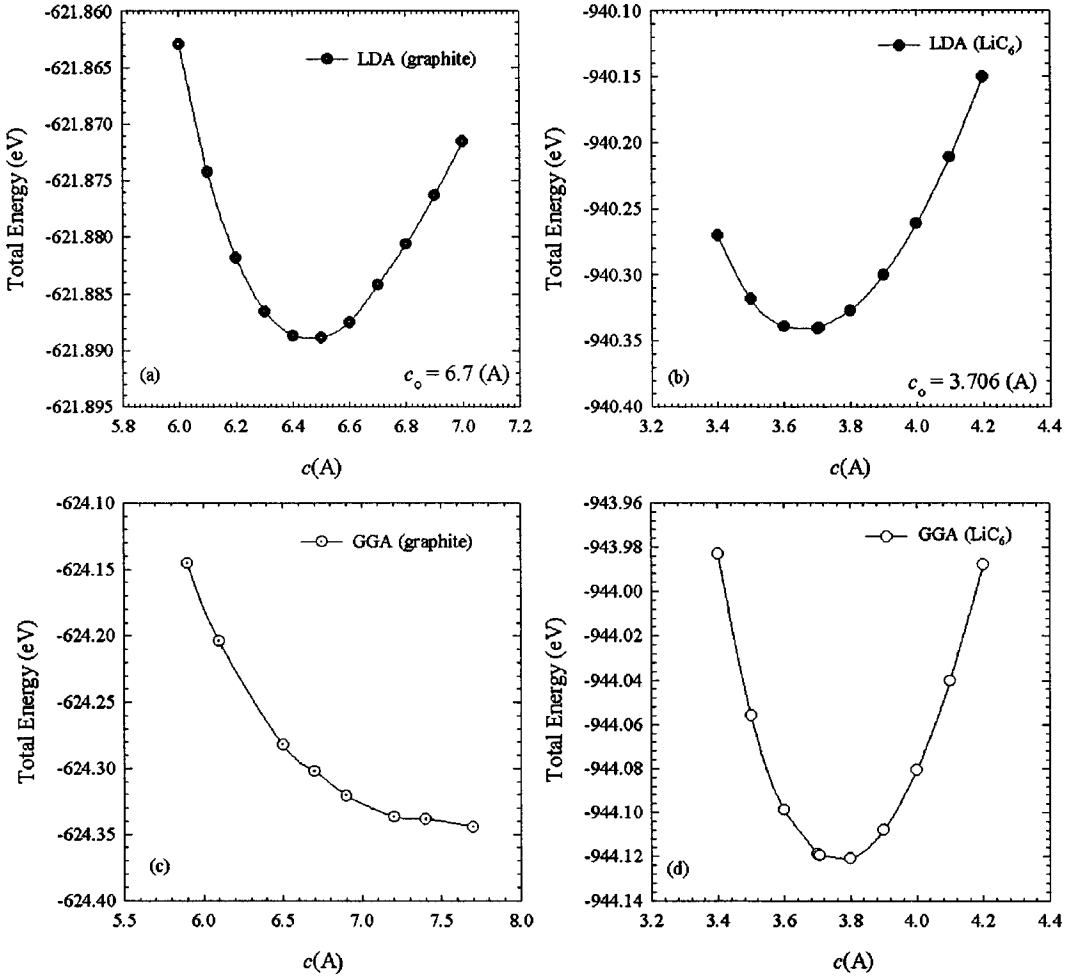

FIG. 3. Lattice parameter c (in angstrom) variation as a function of single-point total energy calculations for graphite and LiC_6. A smooth curve fit in a GGA plot of total energy vs lattice parameter c for graphite and LiC_6.

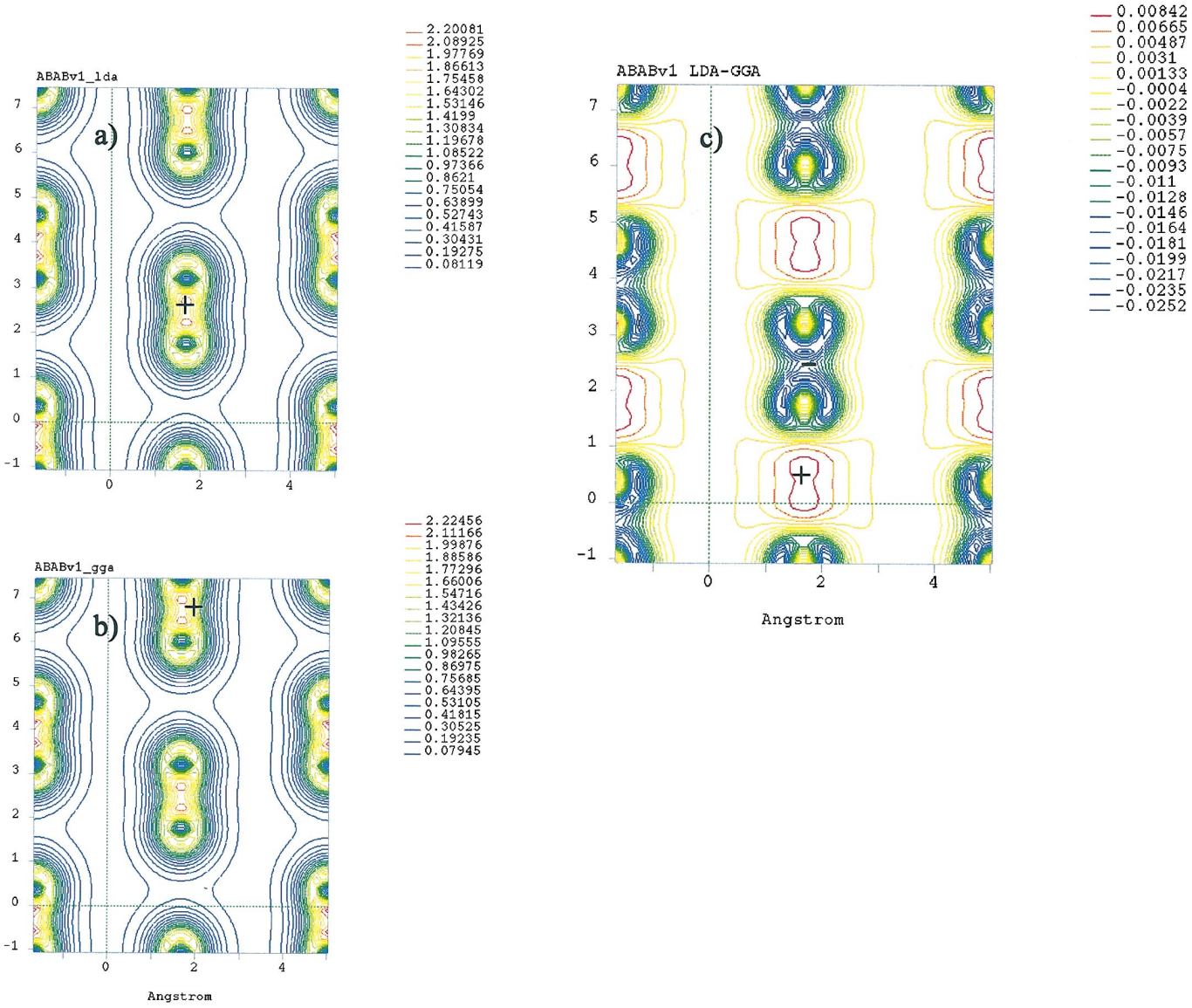

FIG. 4. (Color) Contour plot of the (a) LDA and (b) GGA valence charge density of graphite plotted in a (010) plane which is perpendicular to the graphenes and also features the C-C bond. Contour labels are in units of electrons/Å^3 and vary from $-0.02e$/Å^3 to $\sim 2e$/Å^3. (c) The contour plot of the difference between the LDA and GGA valence electron densities of graphite, plotted in the same plane. Positive and negative zones of electron density are labeled by + and −, respectively.

interlayer bonding, we have subtracted the isolated-graphite-layer electronic density from the graphite electronic density. The LDA calculations [Fig. 5(a)] show that the electronic charge in the neighborhood of the α atoms is depleted along the *c*-axis direction, in agreement with previous results.[55] These electrons are transferred to the neighborhood of the β atoms and also between the *A* and *B* layers. The latter increase of charge, which extends homogeneously in the entire interplanar region, contributes towards the weak van der Waals bonding. Consequently, the LDA predicts the *c* lattice parameter of graphite reasonably well, as shown in Table I. For the GGA calculations [Fig. 5(b)], almost no gain or loss of electrons is shown on α and β atoms in the *B* layer. A depletion of electrons is shown on both α and β atoms in the *A* layer with significant charge residing in the bond between the two atoms. There is no delocalization of electrons between the *A* and *B* layers, resulting in almost no bonding between the layers. This perhaps explains why the GGA fails to predict the *c* lattice parameter (see Table I).

Indeed, the charge difference between contributions from the LDA and GGA [Fig. 5(c)] confirms that the pseudocharge density from the LDA is slightly dominant in the interlayer and in the neighborhood of α and β atoms, particularly in the *A* layer. Those of the GGA are dominant in the bonds connecting α and β atoms in the *A* layer. Although the electron charge densities are three orders of magnitude smaller than those of maximum valence densities, they do, however, provide a preliminary explanation on the sticking of layers as described by the LDA and GGA representations of the exchange-correlation energy.

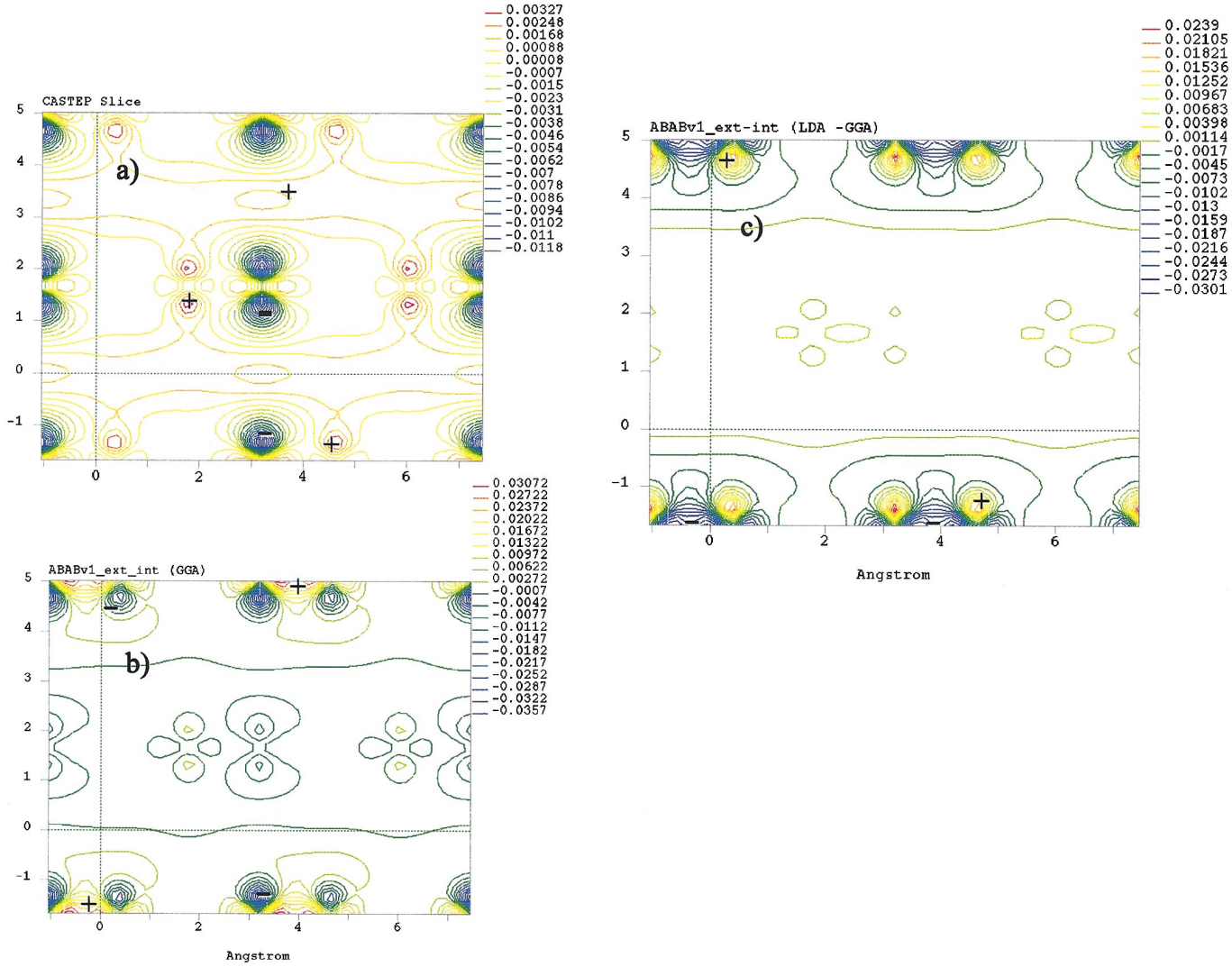

FIG. 5. (Color) Contour plot of the transfer charge due to stacking of graphene layers obtained by the following process: density of graphite minus that of reference graphite layers: **A** plane and **B** plane. Positive and negative zones of electron density are labeled by + and −, respectively. (a) LDA density difference and (b) GGA density difference while (c) is the difference between (a) and (b) as explained in the discussion. Contour labels are in units of electrons/Å^3 and varies from $-0.03e/\text{Å}^3$ to $\sim 0.03e/\text{Å}^3$.

V. HIGH-PRESSURE STUDIES OF GRAPHITE AND LiC_6

Figure 6 shows our calculated pressure-volume equation of state of graphite and related previous experimental results.[5,7,8] The bulk modulus B and its pressure derivative B', obtained from the least-squares fit to the calculated data using Murnaghan equation [Eq. (1)], are given in Table II. Our results compare well with experimental values, in particular, the results of Gauster and Fritz[14] and the theoretical LCGTO-FF results,[58] but appreciably different from FLAPW calculations.[37] The bulk modulus derived from the elastic constants obtained from the GGA-PBE-calculated data, compares impressively well with the experimental result of Zhao and Spain[5] and Blakslee *et al.*,[10] the latter being derived from the elastic constants. Figure 7 shows the relative lattice parameters a/a_0 and c/c_0 of graphite as a function of pressure. In Fig. 7(a), we note that these parameters are nonlinear above approximately 5 GPa. A similar behavior was noted experimentally by Zhao and Spain[5] who mentioned the pres-

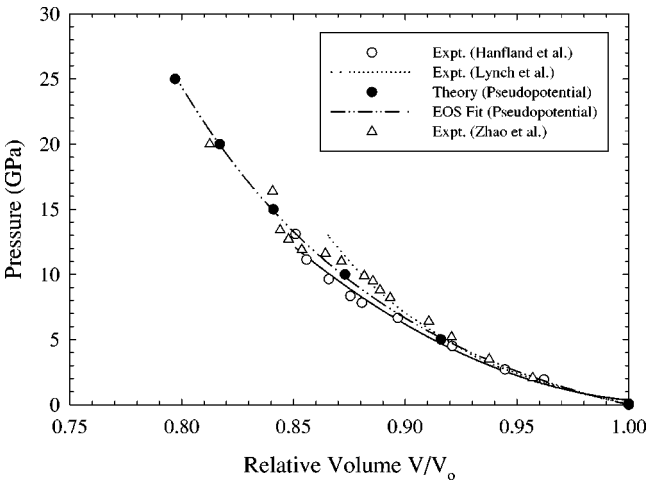

FIG. 6. A comparison of our work (pseudopotential) and experimental (Refs. 5, 7 and 8) equation of state of graphite.

TABLE II. Theoretical and experimental values of the bulk modulus B of graphite.

	B_0 (GPa)	B'
Theory (EOS, LDA)	40.8	7.73
Theory (elastic constants, GGA-PBE)	35.7	
Theory (FLAPW)[a]	50.2	
Theory (LCGTO-FF)[b]	38.3	
Expt. (300 K, elastic constants)[c]	35.8	
Expt. (300 K, elastic constants)[d]	41.0	
Expt. (~0 K, elastic, $P>15$ GPa)[e]	36.0	
Expt. ($20\leqslant$GPa)[f]	35.8	
Expt. (300 K, $P\leqslant 14$)[g]	33.8	

[a]Reference 37.
[b]Reference 58.
[c]Reference 10.
[d]Reference 14.
[e]Reference 7.
[f]Reference 5.
[g]Reference 8.

ence of a phase transition at ~11 GPa. In addition, Clarke and Uher[93] reported that hexagonal graphite transforms to a new phase of carbon, at roughly 15 GPa (increasing pressure), which is likely to be the sp^3-bonded hexagonal form of diamond (wurtzite analog or ''lonsdalite''). The nonlinearity in our results above 5 GPa could be ascribed to a similar transformation.

The one-dimensional analog of the Murnaghan equation[94] provides an approximation for describing the nonlinear relation between normalized lattice parameters and pressure P:

$$r/r_0=\left[\left(\frac{B'}{B_0}\right)P+1\right]^{-1/B'}. \tag{1}$$

Here r is the lattice constant along one of the crystal axes, $\kappa=B^{-1}=-(\partial \ln r/\partial P)$ is the linear compressibility, and B' is the pressure derivative of B (i.e., $\partial B/\partial P$). Therefore, considering the contraction of the c axis, the compressibility of the c axis is defined as

$$\kappa_c=\frac{1}{c_0}\left(\frac{\partial c}{\partial P}\right)_{P_0}, \tag{2}$$

where c is the c-axis lattice constant and c_0 is the c-axis lattice constant at the reference pressure P_0. Note that our calculations are done at ~0 K; hence some caution is necessary when we make a comparison with experimental data.

Table III shows the calculated and experimental linear moduli (B_a and B_c) for graphite, deduced from Fig. 7. Our calculated modulus B_c along the c axis is in good agreement with experimental results from x-ray measurements using powder samples,[7,8,95] single crystals,[96] polycrystalline graphite,[5] and also with adiabatic values derived from the measured elastic constants.[4,10] B_c derived from the calculated elastic constants using Eq. (5) is also in good agreement with experiment.[5,10] Zhao and Spain[5] observed a somewhat c-axis parameter softening at about 10 GPa.

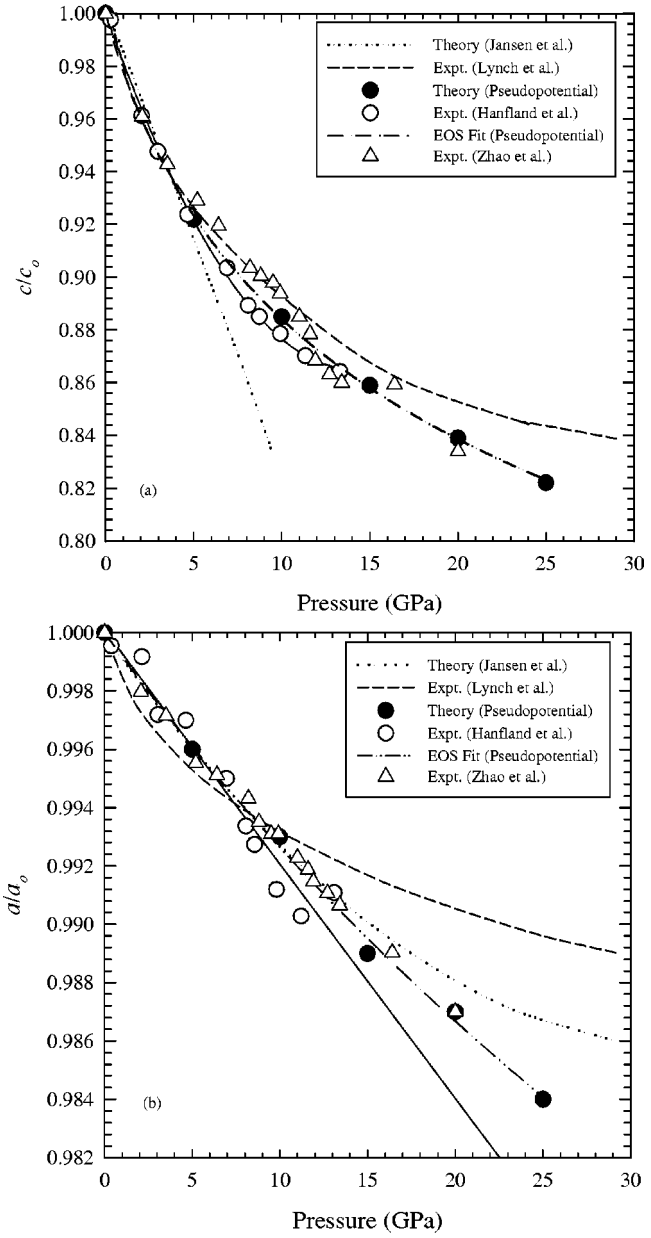

FIG. 7. A comparison of our work (pseudopotential) and calculated (Ref. 37) and experimental (Refs. 5, 7 and 8) values of the relative lattice parameters a/a_0 and c/c_0 of hexagonal graphite as a function of pressure.

Our calculated a-axis modulus B_a compares well with the x-ray results of Hanfland *et al.*[8] and Zhao and Spain,[5] but the calculated B_a from elastic constants of graphite by Blakslee *et al.*[10] is significantly higher (see Table III), in contrast to our calculated B_a from elastic constants. The x-ray diffraction data[7] yielded a much lower value for B_a and a pronounced nonlinearity (large B_a') for the a-axis compression (see Fig. 7). It has been suggested that the nonlinear behavior arises from the onset of buckling or puckering of the graphite layers at low pressures. The x-ray results of Hanfland *et al.*[8] and Zhao and Spain[5] and our results are not consistent with this pronounced nonlinearity. Hence we also find no indica-

TABLE III. First- and second-order axial compression coefficients of graphite. B_0^{-1} is the linear compressibility at zero pressure and B' is the pressure derivative of B.

	B_c (GPa)	B_a (GPa)	B_c' (GPa)	B_c' (GPa)
Theory (EOS, LDA)	40.6	1206	10.2	30.6
Theory (elastic constants, GGA-PBE)	37.0	874		
Expt. (x-ray, $P \leqslant 20$ GPa)[a]	37.0	1580		
Expt. (300 K, x-ray, $P \leqslant 14$ GPa)[b]	35.7	1250	10.8	
Expt. (300 K, x-ray, $P > 15$ GPa)[c]	35.0	640	14	210
Expt. (x-ray, $P \leqslant 1.6$ GPa)[d]	35.7			
Expt. (x-ray, $P \leqslant 1.6$ GPa)[e]	36.6			
Expt. (elastic constants)[f]	37.3	2000		
Expt. (elastic constants)[g]	34.0			

[a]Reference 5.
[b]Reference 8.
[c]Reference 7.
[d]Reference 95.
[e]Reference 96.
[f]Reference 10.
[g]Reference 4.

tion for a significant puckering or buckling of the graphite layers during the initial compression. The compressibility measurements for graphite along the c axis (package thickness) is reported to be $\kappa_c = (2.73 \pm 0.09) \times 10^{-12}$ cm^2/dyn (Ref. 96) for hydrostatic pressure $\leqslant 10$ kbar and $\kappa_c = (2.79 \pm 0.1) \times 10^{-12}$ cm^2/dyn (Ref. 97). This compares very well with our calculated c-axis compressibility $\kappa_c = 2.46 \times 10^{-2}$ (GPa^{-1}) considering that our calculations are carried out at ~ 0 K for hydrostatic pressure $\leqslant 25$ GPa.

At lower volumes, graphite is best described as being quasi two dimensional, but for very high pressures it is rapidly transforming to a more isotropic material. To compare meaningfully with experiments at high pressure, it is necessary to consider c/a values along the hydrostatic curves in Figs. 8 and 9. The calculated c/a ratio of graphite derived from the latter calculation is displayed in Fig. 8 and compared with experimental data[5,8] at pressures up to about 14 GPa. Our pseudopotential calculation slightly underestimates the c/a compressibility though the agreement with experiments is reasonable. The c/a values are also plotted as a function of relative volume in Fig. 9, along with experimental data of Zhao and Spain,[5] FLMTO results of Ahuja *et al.*,[49] and earlier Boettger[58] pseudopotential results. The c/a values obtained here form a smooth line that lies slightly below the experimental data and steadily converges with that data as the volume is reduced.

We now discuss the hydrostatic pressure response of LiC_6. Figure 10(a) shows a plot of pressure against the relative volume and (b) a variation of the relative volume as a function of c/a ratio, where V_0 is the volume of the geometrically optimized structure at 0 GPa. The curve is fitted to Eq. (1) and yields the total bulk modulus of $B_0 = 66.75$ GPa and $B' = 5.32$ (see Table IV). The bulk modulus is higher than that of graphite, similar to the trends of B_0 derived from the calculated elastic constants, hence suggesting LiC_6 to be harder. The P-V curve is relatively more linear as compared to that of graphite. Figures 11(a) and 11(b) show plots of relative lattice parameters a/a_0 and c/c_0 as a function of pressure. These plots are fitted to a Murnaghan[94] equation of state from which we extract linear bulk moduli $B_c = 74.38$ GPa ($B_c' = 6.92$) and $B_a = 1190.15$ GPa ($B_a' = 28.74$). The latter value, derived from Fig. 11(b), confirms nonlinearity (large B_a') for the a-axis compression observed in graphite. This value is slightly lower than that of graphite, confirming the larger hexagonal ring in LiC_6, which is 3 times larger in area than that of graphite. B_c and B_a calculated from the elastic constants using Eqs. (5) and (6) shows an increase in B_c with almost

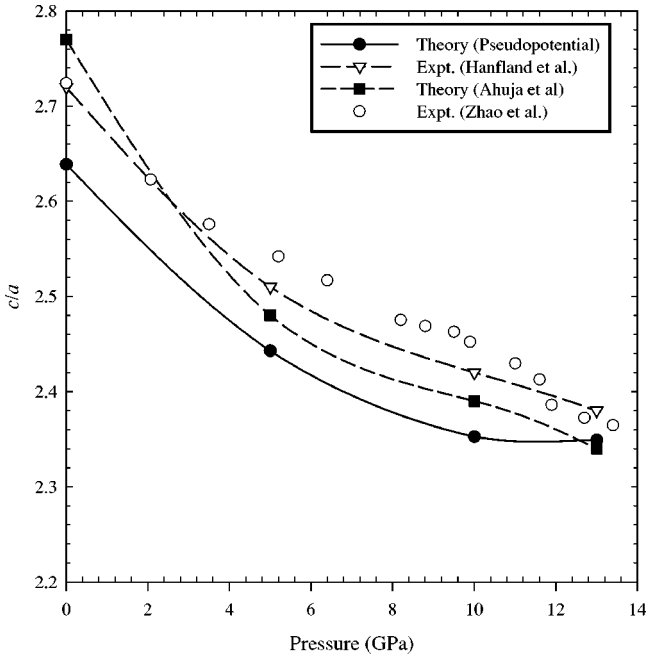

FIG. 8. A comparison of our work (pseudopotential) and experimental (Refs. 5 and 8) values of c/a ratio of hexagonal graphite as a function of relative volume.

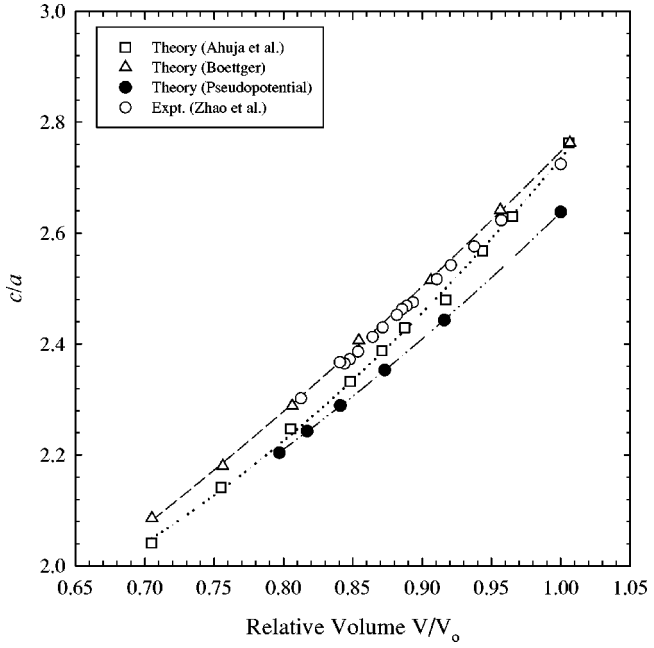

FIG. 9. A comparison of our work (pseudopotential), calculated (Refs. 49 and 58) and experimental (Ref. 5) values c/a ratio of hexagonal graphite as a function of relative volume.

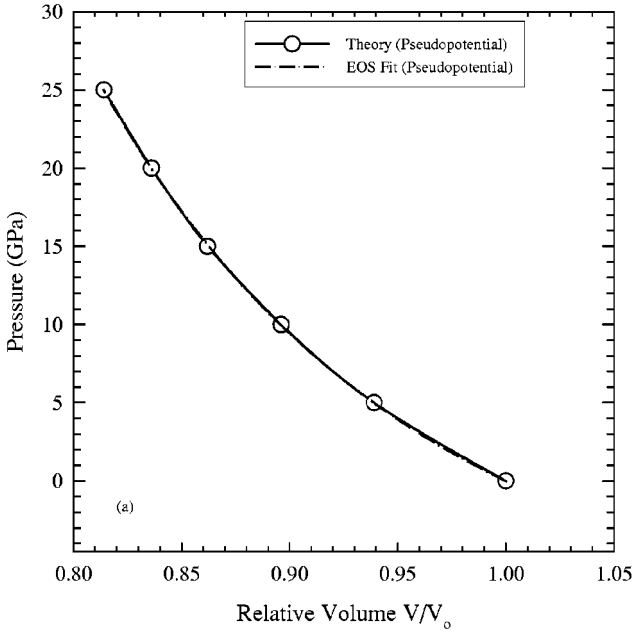

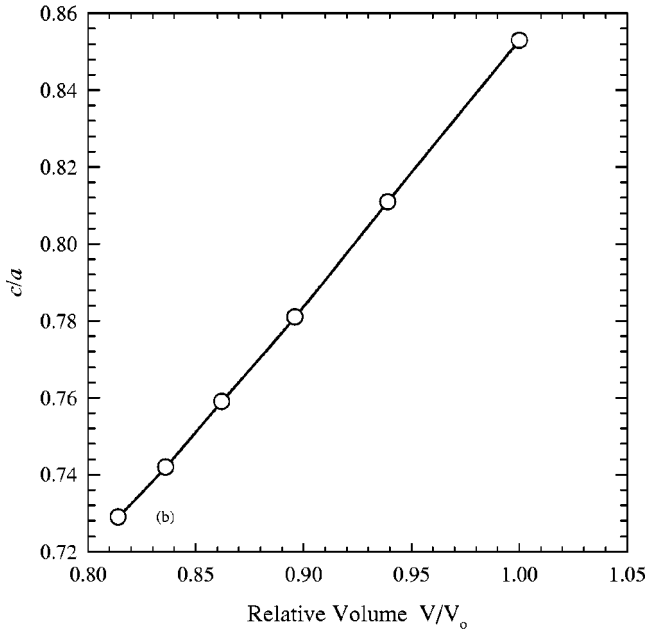

FIG. 10. A plot of the equation of state (a) for LiC_6 and (b) a variation of the relative volume as a function of c/a ratio.

no change in B_a when comparing graphite and LiC_6. We have also plotted $\ln(c/c_0)$ versus pressure [Fig. 11(a), inset] in order to compare our results with experimental work of Zhou and Fischer,[33] where the linear change at low pressures is well reproduced.

In Table IV our calculated linear moduli and compressibility are compared with experimental[33,68,69] data. Neutron diffraction measurements[33] reported the c-axis compressibility for LiC_6 at 300 K to be $\kappa_c=(1.43\pm0.02)\times10^{-12}$ cm^2/dyn [$\kappa_c=(1.43\pm0.02)\times10^{-2}$ GPa^{-1}] for hydrostatic pressure $\leqslant$2.3 GPa. This compares very well with our calculated c-axis compressibility $\kappa_c=1.344\times10^{-2}$ (GPa^{-1}) considering that our calculations are carried out at $\sim$0 K for hydrostatic pressure $\leqslant$25 GPa. There is a notable decrease by 83% in the c-axis compressibility relative to graphite, implying that the interlayer coupling in LiC_6 is stronger. Earlier measurements[68] on LiC_6, using ^{7}Li NMR spectra and the point charge model predicted κ_c to be 1.7×10^{-12} cm^2/dyn [$\kappa_c=(1.7\pm0.02)\times10^{-2}$ GPa^{-1}] for pressures ranging from 1.7×10^{-4} to 0.5 GPa, at $T=232$ K. This compares well with $\kappa_c=1.65\times10^{-2}$ GPa^{-1}, derived from the elastic constants calculations. Nalimova *et al.*[70] also reported compressibilities of 3.56×10^{-3} and 2.64×10^{-3} kbar^{-1} for LiC_6 in the ranges 0–10 and 0–20 kbar, respectively.

The calculated variation of the anisotropy, c/a, of LiC_6 with hydrostatic pressure is given in Fig. 10. The plot is linear, signifying uniform compression in LiC_6. In an anisotropic crystal structure such as LiC_6, one would expect the compressibility parallel $\kappa_a=8.40\times10^{-4}$ (GPa^{-1}) and perpendicular $\kappa_c=1.344\times10^{-2}$ (GPa^{-1}) to the layer planes to be very different. The coplanar covalent bonds of carbon atoms are so strong that the in-plane contraction at lower pressures can be neglected.[98] We note a very small difference in the compressibility along the a axis for graphite [$\kappa_a=8.29\times10^{-4}$ (GPa^{-1})] and LiC_6.

VI. ELASTIC CONSTANTS

Hexagonal graphite and LiC_6 crystals have six different elastic coefficients where the elastic constant tensor [C_{ij}] contains only 5 independent constants instead of 21 in the general case:

TABLE IV. Theoretical values of the bulk modulus B_0 and a comparison of the calculated and experimental first- and second-order axial compression coefficients of LiC_6.

	B_0 (GPa)	B'	B_c (GPa)	B_a (GPa)	κ (10^{-2} GPa^{-1})	κ_c (10^{-2} GPa^{-1})	κ_a (10^{-2} GPa^{-1})
Theory (EOS, LDA)	66.75	5.32	74.38	1190.15	1.50	1.34	0.084
Theory (elastic constants, GGA-PBE)	56.51		60.56	875.97	1.77	1.65	
Expt.[a]						1.70	
Expt.[b]						1.43 ± 0.02	
Expt.[c]						1.43 ± 0.01	

[a]Reference 68.
[b]Reference 33.
[c]Reference 69.

$$[C_{ij}]=\begin{bmatrix} C_{11} & C_{12} & C_{13} & 0 & 0 & 0 \\ C_{12} & C_{11} & C_{13} & 0 & 0 & 0 \\ C_{13} & C_{13} & C_{33} & 0 & 0 & 0 \\ 0 & 0 & 0 & C_{44} & 0 & 0 \\ 0 & 0 & 0 & 0 & C_{44} & 0 \\ 0 & 0 & 0 & 0 & 0 & C_{66} \end{bmatrix}, \quad (3)$$

with $C_{66}=\frac{1}{2}(C_{11}-C_{12})$, associated with the order parameter. The elastic constant tensor is related to the stress σ and strain ϵ by the following equation:

$$\sigma_i=\sum_{j=1}^{6} C_{ij}\epsilon_{ij}, \quad (4)$$

where i and j represent the six unequal combinations of three axes (x, y, and z).

The elastic properties are used to quantify the crystalline bonding strength or stiffness in specific direction. C_{11} and C_{33} are the longitudinal moduli, where C_{33} is the interlayer stiffness in the c direction, while the C_{44} and C_{66} are the shear moduli. $C_{11}+C_{12}$ in graphite is the intralayer stiffness in the directions parallel to the AB plane [see Fig. 1(a)]. C_{12} and C_{13} are the mixed-index moduli, with C_{13} being the stiffness in linear combination of the direction along the c axis and the directions parallel to the AB plane.

The formulas for the bulk modulus along the a and c axes, i.e., linear moduli B_a and B_c in terms of the elastic stiffness constant C_{ij}, are

$$B_c=c_0\frac{dP}{dc}=\frac{B_a}{\beta}, \quad (5)$$

$$B_a=a_0\frac{dP}{da}=\frac{\delta}{(1+\alpha+\beta)}, \quad (6)$$

where

$$\delta=C_{11}+2C_{12}\alpha+2C_{13}\beta+C_{33}\beta^2+2C_{13}\alpha\beta. \quad (7)$$

For hexagonal systems,

$$\alpha=1, \quad \beta=\frac{C_{11}+C_{12}-2C_{13}}{C_{33}-C_{13}}. \quad (8)$$

Table V gives a complete set of calculated elastic constants of graphite and LiC_6, and these are compared with available experimental results. Due to the large anisotropy in graphite, most properties are mainly determined by $C_{11}+C_{12}$ and to a smaller extent by C_{33}; C_{13} does not play a significant role.[37] C_{11} of graphite, calculated using the LDA and GGA-PBE, agrees very well with ultrasonic measurements[15] and some of the previous theoretical calculations,[39,40,99] though neutron scattering results, which tend to have appreciable errors, have a deviation of 28%. C_{12}, from the LDA calculations, is consistent with the experimental result of Seldin and Nezbeda,[15] while the GGA calculations underestimate the value by 5%. $C_{11}+C_{12}$ compares well with experimental results[10,15] with an error margin of 2%. The C_{33} value from the GGA calculation agrees well with the experimental value[14] at $\sim$0 K, and is closer to ultrasonic[10,15] and neutron[20] measurements within a 10% error margin. The LDA value of $C_{44}=1.24\pm0.5$ GPa, which is closer to the ultrasonic measurements,[10,13,15] which range from 0.25 to 1.2 GPa. Neutron[20,21] and Brillouin[100] scattering techniques and, on the other hand, yield values of 4.6 ± 0.2, 3.84 ± 0.4, and 5.05 ± 0.35 GPa for graphite, respectively. The GGA-PBE value of 3.28 ± 0.5 GPa agree better with the neutron scattering result,[20] which according to Kelly[34] is expected to be more reliable because it is consistent with specific heat data. From Table V, C_{13} is the only calculated elastic constant with a negative value and the experimental value is positive.[15] The negative value of C_{13} indicates that there is a complicated response of the system to uniaxial stress.

As noted in Table V, the experimental and theoretical elastic constants of LiC_6 are scarce; consequently, our results present the first complete set. There is generally a good correspondence between the LDA and GGA-PBE results. C_{11} compares reasonably with previously calculated value[40] where it deviates by 7%. Our GGA-PBE-calculated C_{33} value is within 6% of the experimental value of Fischer and co-workers,[33,69] while it departs from the data of Zabel *et al.*[101] by 26%. The strong interaction in LiC_6 has led to a

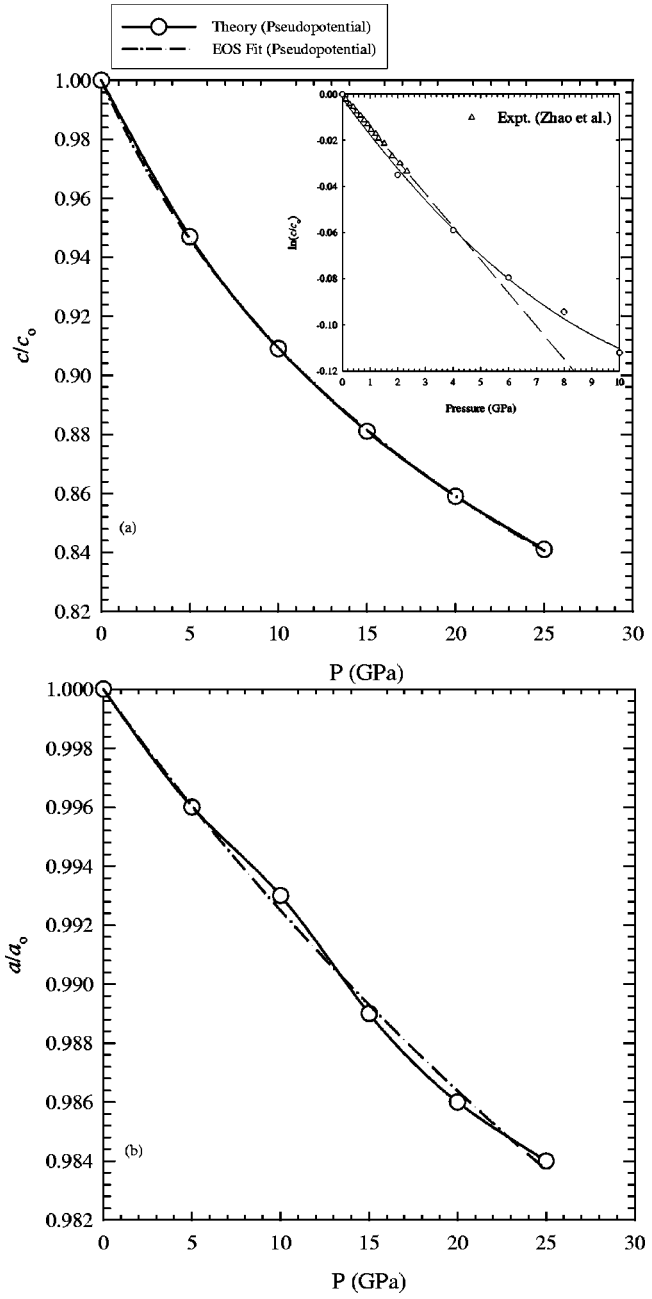

FIG. 11. Relative latice parameters a/a_0 and c/c_0 of LiC_6 as a function of pressure. Inset: calculated and experimental (Ref. 33), pressure dependence of the (normalized) LiC_6 lattice parameter c.

31% increase of C_{33} as compared to graphite. C_{13} is negative, as in graphite, and hence this sign can be ascribed to similar reasons advanced for graphite. We further note that lithium intercalation has almost reduced C_{13} of graphite by half. Our calculated $C_{44}=16.98$ GPa compares well with experimental results of Kamitakahara[102] who reported $C_{44}=(17.3\pm1.0)\times10^{10}$ dyn/cm^2 and depicts a significant departure from the data of Zabel *et al.*[101] who reported $C_{44}=(10.0\pm1.0)\times10^{10}$ dyn/cm^2. In addition our calculated C_{44} agrees reasonably with the data by Lang *et al.*,[40] where $C_{44}=15.0$ GPa. The shear modulus C_{44} of LiC_6 is significantly larger than that of graphite. Shear resistance in the layers reflects the strong ionic bond between intercalant and host layers. There is a notable reduction in $C_{11}+C_{12}$ compared to graphite, which can be ascribed to the expansion in the C-C bond length in LiC_6.

$C_{12}\neq C_{66}$ and $|C_{13}|\neq C_{44}$, which clearly shows that graphite and LiC_6 do not obey the Cauchy relations. The planar Young's moduli of graphite and LiC_6 are 974.93 and 877.35 GPa, respectively, while in the c-axis direction they are 11.38 and 52.11 GPa. These results confirms that the compressibility of graphite is highly anisotropic. Kelly[35] reported the experimental value of 1020 and 37 GPa for graphite in the plane and along the c axis, respectively.

VII. DENSITY OF STATES

Figure 12(a) shows the calculated valence band of the total DOS of graphite, determined using the linear interpolation scheme,[104] with the Gaussian broadening width of 0.5 eV. The experimental results, given in Fig. 12(b), were obtained by x-ray photoemission spectroscopy, with energetic photons of 122 eV (the experimental broadening is estimated at 0.4 eV).[18] The two-dimensional character of graphite is confirmed by the form of the DOS, which increases suddenly from zero to a near constant value, above -23 eV, instead of increasing as the square root of the energy, which is the behavior of the density of states for free electrons in three dimensions. A deep pseudogap occurs at the Fermi level. In general, it can be concluded that our calculations reproduce the experimental DOS well. Figure 13(a) depicts a comparison of the total DOS for graphite and LiC_6. They generally have similar peaks except for the shifting of related peaks to lower energies in both the valence and conduction bands observed in LiC_6.

Figure 13(b) shows the total and partial electron density of states for the Li ion in LiC_6, with the Gaussian broadening width of 0.05 eV. The valence band of graphite and LiC_6 consists of the s and p orbitals of α carbons, with the s component dominating at lower energies (-24 to -12 eV) and the p component being more pronounced at higher energies closer to the Fermi level. The contribution of the Li ion to the total DOS is from the s orbital only, which appears at very low energies in the conduction band, indicating insignificant bonding with the carbon atoms. The contributions of the s and p orbitals of the α carbon atoms are, on the whole, similar to those of carbon in graphite, except that their associated features are shifted to lower energies. Graphite is semimetallic with a very low density of states at E_F. In LiC_6 the presence of the Li ion raises E_F (by contributing one conduction electron), thereby giving rise to a large DOS at E_F [see Fig. 13(a)].

The experimental results for the PDOS of graphite and the total DOS and PDOS for LiC_6 are not available. However, in view of an excellent agreement between our calculated and the experimental DOS of graphite [see Figs. 12(a) and 12(b)], it can be surmised that the predicted total DOS and PDOS for LiC_6 [see Figs. 13(a) and 13(b)] are accurate enough.

TABLE V. Elastic constants for graphite and LiC_6 (in GPa).

Graphite	C_{11}	C_{12}	C_{13}	C_{33}	C_{44}	C_{66}	$C_{11}+C_{12}$
Theory (this work, GGA-PBE)	1036.3±2.4	170.3±1.4	−12.4±0.2	39.8±0.6	3.3±0.5	432.9	1206.6
Theory (this work, LDA)	1037.7±2.4	180.8±1.6	−12.4±0.3	22.7±0.6	1.2±0.5	428.4	1218.5
Expt. (300 K)[a]	1060.0		40.0	36.0			1240.0
Expt. (0 K)[b]			15.0	41.0			1330.0
Expt.[c]	1060.0	180.0	15.0	36.5	4.5	440.0	1240.0
Expt.[d]	1440.0			37.1	4.6	460.0	
Expt.[e]					3.84±0.4		
Expt.[f]					5.05		
Expt.[g]					3.84		
Expt.[h]	950.0					420.0	
Theory[i]	1130.0			37.4	4.4	388.0	
Theory[j]	1060.0		15.0	36.9	4.2	450.0	
Theory[k]	1450.0		−0.6	36.5	0.6	440.0	
Theory[l]							1250.0
Theory (FLAPW)[m]			−12.0±0.13	56.0±0.09			1430.0±1.7
LiC_6							
Theory (this work, LDA)	897.5±2.6	131.7±0.2	−7.9±0.5	52.2±1.0	17.0±0.2	382.93	1029.2±1.4
Theory (this work, GGA-PBE)	900.5±1.8	119.8±0.5	−6.2±0.4	65.2±1.3	17.9±0.2	390.3	1020.3±1.1
Theory[i]	747.0			47.1	15.0	391.0	
Expt.[n]				88.6	10.0		
Expt.[o]				69.7			
Expt.[g]					17.3		
Expt.[p]				69.3			

[a]Reference 10.
[b]Reference 14.
[c]Reference 15.
[d]Reference 20.
[e]Reference 21.
[f]Reference 100.
[g]Reference 102.
[h]Reference 103.
[i]Reference 40.
[j]Reference 39.
[k]Reference 99.
[l]Reference 63.
[m]Reference 37.
[n]Reference 101.
[o]Reference 33.
[p]Reference 69.

VIII. CONCLUSION

In conclusion, the lattice parameters of graphite and LiC_6 have been calculated within the LDA and GGA approximations. The *a* and *c* lattice parameters for both compounds were well reproduced, except for the *c* value of graphite by the GGA, since this approximation does not represent the weak interactions between the carbon layers of graphite well. The electronic charge differences of the two compounds were calculated within the LDA and GGA, and explained the failure of the GGA to reproduce the *c* parameter in graphite. GGA theory does give a reliable description of LiC_6 and therefore may be relied upon in studies of Li-intercalated graphite. LDA calculations are generally known to produce shorter bond lengths and consequently higher bulk moduli. High-pressure calculations were carried out on graphite and LiC_6 and bulk moduli decided from equations of state agreed well with experimental results. Our results also confirms that GIC's have a greater compressibility along the *c* axis as compared with graphite: hence, the hydrostatic pressure also acts on LiC_6 uniaxially

Anisotropic features in graphite and LiC_6 were also explained from these studies. A discrepancy of ~20% in the experimental value of the axial compression coefficient was found from Refs. 33 and 68. Our results are in agreement with the experimental value reported by McClure[41] within 6%, hence resolving the discrepancy found in the literature. The predicted elastic constants have provided a complete set of elastic constant for graphite and LiC_6. Furthermore, good

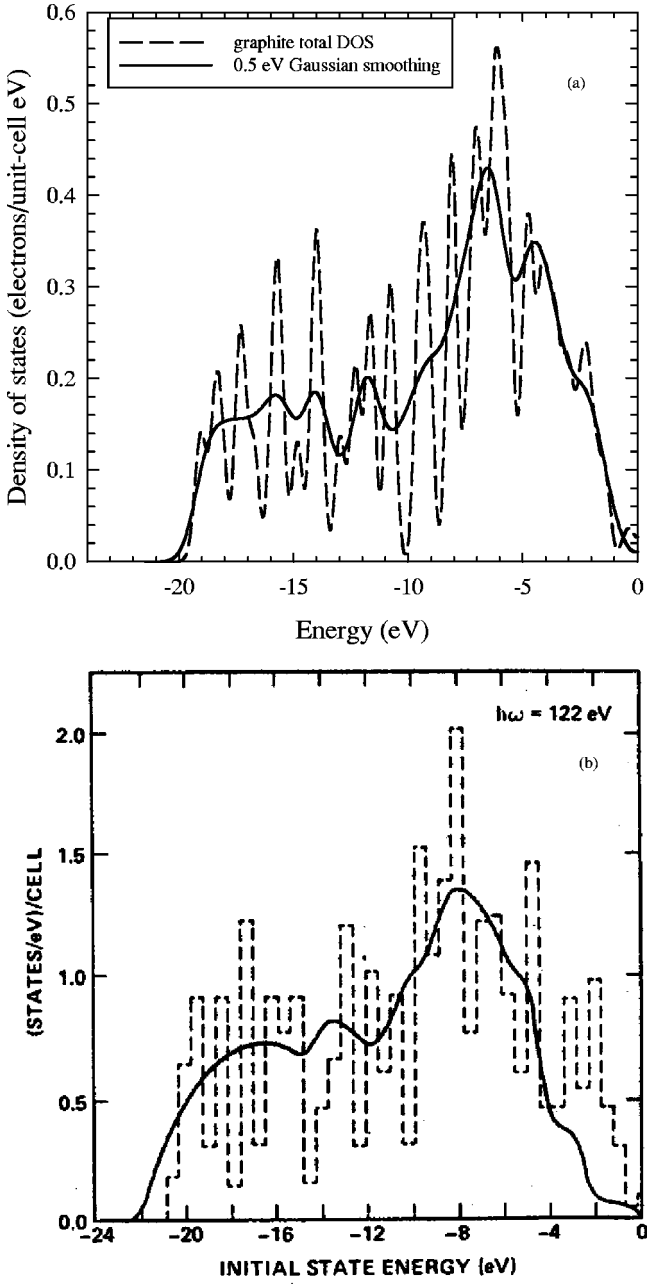

FIG. 12. Comparison of graphite (a) theoretical DOS and theoretical smoothed interpolated DOS, with the Gaussian broadening width of 0.5 eV. (b) Experimental x-ray photoemission spectra (Ref. 18).

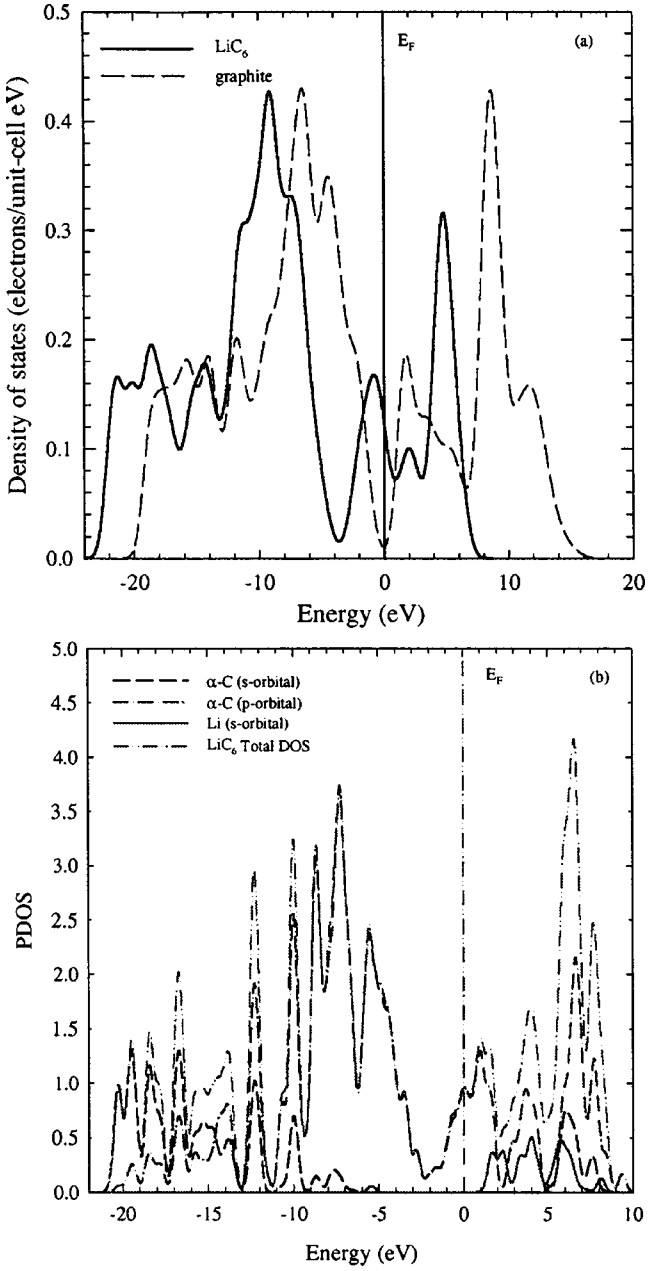

FIG. 13. (a) A comparison of the calculated total density of states for graphite and LiC_6. (b) Total and partial electron density of states for the Li ion and α carbons in the graphitic layer in LiC_6. The Fermi level E_F is set at zero.

agreement with most available experimental data and other theoretical results has been demonstrated. The shear constants are larger in LiC_6 than in pure graphite, although it has been reported[21] that they are smaller in other stage-1 compounds. Total DOS of graphite and LiC_6 were calculated and provided useful insights into the bonding of atoms in these compounds, particularly the delocalization of the Li ion in LiC_6. There is a notable lack of experimental high-pressure structural parameters and electronic properties, such as density of states, in LiC_6. Hence it will be valuable if such work can be carried out and be compared with our calculations.

ACKNOWLEDGMENTS

We would like to acknowledge the National Research Foundation (NRF) and Royal Society (UK) for financial support of the execution of this work. We are also grateful to the Materials Modelling Center for the availability of computational facilities at the University of the North.

*Also at Materials and Manufacturing Technology, Council for the Scientific and Industrial Research, Pretoria, 0001, South Africa. Electronic address: ngoepep@unorth.ac.za

[1] G. S. Painter and D. E. Ellis, Phys. Rev. B **1**, 4747 (1970).
[2] R. F. Willis, B. Feuerbacher, and B. Fitton, Phys. Rev. B **9**, 2441 (1974).
[3] J. R. Darn *et al.*, in *Lithium Chemistry Library*, edited by G. Pistoia (Elsevier, Amsterdam, 1994), Vol. 5, p. 1.
[4] B. Alzyab, C. H. Perry, C. Zahopoulos, O. A. Pringle, and R. M. Nicklow, Phys. Rev. B **38**, 1544 (1988).
[5] Y. X. Zhao and I. L. Spain, Phys. Rev. B **40**, 993 (1989).
[6] T. Yagi, W. Utsumi, M. A. Yamakata, T. Kikegawa, and O. Shimomura, Phys. Rev. B **46**, 6031 (1992).
[7] R. M. Lynch and H. G. Drickamer, J. Chem. Phys. **44**, 181 (1966).
[8] M. Hanfland, H. Beister, and K. Syassen, Phys. Rev. B **39**, 12 598 (1989).
[9] M. Hanfland, K. Syassen, and R. Sonnenschein, Phys. Rev. B **40**, 1951 (1989).
[10] O. L. Blakslee, D. G. Proctor, E. J. Seldin, G. B. Spence, and T. Wing, J. Appl. Phys. **41**, 3373 (1970).
[11] G. B. Spence *et al.*, J. Appl. Phys. **41**, 3383 (1970).
[12] F. Tuinstra and J. L. Koenig, J. Chem. Phys. **53**, 1126 (1970).
[13] W. B. Gauster, Philos. Mag. **25**, 687 (1972).
[14] W. B. Gauster and I. J. Fritz, J. Appl. Phys. **45**, 3309 (1974).
[15] E. J. Seldin and C. W. Nezbeda, J. Appl. Phys. **41**, 3389 (1970).
[16] D. A. Fischer, R. M. Wentzcovitch, R. G. Carr, A. Continenza, and A. J. Freeman, Phys. Rev. B **44**, 1427 (1991).
[17] T. L. Schindler and Y. K. Vohra, J. Phys.: Condens. Matter **7**, L637 (1995).
[18] A. Bianconi, S. B. M. Hagstrom, and R. Z. Bachrach, Phys. Rev. B **16**, 5543 (1977).
[19] G. Bellodi, A. Borghesi, G. Guizzetti, L. Nosenzo, E. Reguzzoni, and G. Samoggia, Phys. Rev. B **12**, 5951 (1975).
[20] R. Nicklow, N. Wakabayashi, and H. G. Smith, Phys. Rev. B **5**, 4951 (1972).
[21] H. Zabel, W. A. Kamitakahara, and R. M. Nicklow, Phys. Rev. B **26**, 5919 (1982).
[22] W. Eberhardt, I. T. McGovern, E. W. Plummer, and J. E. Fischer, Phys. Rev. Lett. **44**, 200 (1980).
[23] A. R. Law, J. J. Barry, and H. P. Hughes, Phys. Rev. B **28**, 5332 (1983).
[24] T. Takahashi, H. Tokailin, and T. Sagawa, Phys. Rev. B **32**, 8317 (1985).
[25] V. Dose, G. Reusing, and H. Scheidt, Phys. Rev. B **26**, 984 (1982).
[26] Th. Fauster, F. J. Himpsel, J. E. Fischer, and E. W. Plummer, Phys. Rev. Lett. **51**, 430 (1983).
[27] D. Marchand, C. Fretigny, M. Lagues, F. Batallan, C. Simon, I. Rosenman, and R. Pinchaux, Phys. Rev. B **30**, 4788 (1984).
[28] R. Claessen, H. Carstensen, and M. Skibowski, Phys. Rev. B **38**, 12 582 (1988).
[29] I. R. Collins, P. T. Andrews, and A. R. Law, Phys. Rev. B **38**, 13 348 (1988).
[30] F. Maeda, T. Takahashi, H. Ohsawa, S. Suzuki, and H. Suematsu, Phys. Rev. B **37**, 4482 (1988).
[31] Ch. Byreuther and G. Wiech, in *Extended Abstracts of the Fourth International Conference on VUV-Radiation Physics*, edited by E. E. Kock, R. Haensel, and C. Kunz (Pergamon, Vieweg, 1974), p. 517.
[32] J. Kieser, Z. Phys. B **26**, 1 (1977).
[33] P. Zhou and J. E. Fischer, Phys. Rev. B **53**, 12 643 (1996).
[34] B. T. Kelly, High Temp. - High Press. **13**, 245 (1981).
[35] B. T. Kelly, *The Physics of Graphite* (Applied Science Publishers, London, 1981).
[36] J. F. Green and I. L. Spain, Phys. Rev. B **11**, 3935 (1975).
[37] H. J. F. Jansen and A. J. Freeman, Phys. Rev. B **35**, 8207 (1987).
[38] C. T. Chan, K. M. Ho, and W. A. Kamitakahara, Phys. Rev. B **36**, 3499 (1987).
[39] R. Al-Jishi and G. Dresselhaus, Phys. Rev. B **26**, 4514 (1982).
[40] L. Lang, S. Doyen-Lang, A. Charlier, and M. F. Charlier, Phys. Rev. B **49**, 5672 (1994).
[41] J. W. McClure, Phys. Rev. **108**, 612 (1957).
[42] J. C. Slonczewski and P. R. Weiss, Phys. Rev. **109**, 272 (1958).
[43] A. Zunger, Phys. Rev. B **17**, 626 (1978).
[44] D. P. DiVincenzo, E. J. Mele, and N. A. W. Holzwarth, Phys. Rev. B **27**, 2458 (1983).
[45] J. Korringa, Physica **13**, 392 (1947).
[46] W. Kohn and N. Rostoker, Phys. Rev. **94**, 1111 (1954).
[47] R. C. Tatar and S. Rabii, Phys. Rev. B **25**, 4126 (1982).
[48] M. Weinert, E. Wimmer, and A. J. Freeman, Phys. Rev. B **26**, 4571 (1982).
[49] R. Ahuja, S. Auluck, J. Trygg, J. M. Wills, O. Eriksson, and B. Johansson, Phys. Rev. B **51**, 4813 (1995) and references therein.
[50] R. Ahuja, S. Auluck, O. Eriksson, and B. Johansson, J. Phys.: Condens. Matter **9**, 9845 (1997).
[51] R. Ahuja, S. Auluck, J. M. Wills, M. Alouani, B. Johansson, and O. Eriksson, Phys. Rev. B **55**, 4999 (1997).
[52] N. A. W. Holzwarth, S. G. Louie, and S. Rabii, Phys. Rev. B **26**, 5382 (1982).
[53] N.-X. Chen, S. Rabii, and N. A. W. Holzwarth, Synth. Met. **6**, 197 (1985).
[54] D. Tomanek and S. G. Louie, Phys. Rev. B **37**, 8327 (1988).
[55] J.-C. Charlier, X. Gonze, and J.-P. Michenaud, Phys. Rev. B **43**, 4579 (1991).
[56] M. C. Schabel and J. L. Martins, Phys. Rev. B **46**, 7185 (1992).
[57] K. R. Kganyago and P. E. Ngoepe, Mol. Simul. **22**, 39 (1999).
[58] J. C. Boettger, Phys. Rev. B **55**, 11 202 (1997).
[59] J. Furthmuller, J. Hafner, and G. Kresse, Phys. Rev. B **50**, 15 606 (1994).
[60] M. T. Yin and M. L. Cohen, Phys. Rev. B **29**, 6996 (1984).
[61] S. Fahy, S. G. Louie, and M. L. Cohen, Phys. Rev. B **35**, 7623 (1987).
[62] Y.-H. Kim, I.-H. Lee, S. Nagaraja, J.-P. Leburton, R. Q. Hood, and R. M. Martin, Phys. Rev. B **61**, 5202 (2000).
[63] C. T. Chan, W. A. Kamitakahara, K. M. Ho, and P. C. Eklund, Phys. Rev. Lett. **58**, 1528 (1987).
[64] M. Zanini, S. Basu, and J. E. Fischer, Carbon **16**, 211 (1978).
[65] S. Basu *et al.*, Mater. Sci. Eng. **38**, 275 (1979).
[66] U. M. Gubler, P. Oelhafen, and H. J. Güntherodt, Solid State Commun. **44**, 1621 (1982).
[67] G. K. Wertheim, P. M. Th. M. Van Attekum, and S. Basu, Solid State Commun. **33**, 1127 (1980).
[68] C. Marinos, S. Plesko, J. Jonas, J. Conrad, and D. Guerard, Solid State Commun. **47**, 645 (1983).
[69] C. Bindra, V. A. Nalimova, D. E. Sklovsky, W. A. Kamitakahara, and J. E. Fischer, Phys. Rev. B **57**, 5182 (1998).

[70] V. A. Nalimova, D. Guerard, D. E. Sklovsky, and D. Cox, J. Phys. Chem. Solids **57**, 771 (1996).
[71] N. A. W. Holzwarth and S. Rabii, Mater. Sci. Eng. **31**, 195 (1977).
[72] N. A. W. Holzwarth, S. Rabii, and L. A. Girifalco, Phys. Rev. B **18**, 5190 (1978).
[73] N. A. W. Holzwarth, L. A. Girifalco, and S. Rabii, Phys. Rev. B **18**, 5206 (1978).
[74] N. A. W. Holzwarth, S. G. Louie, and S. Rabii, Phys. Rev. B **28**, 1013 (1983).
[75] R. Chen, P. Truncano, and R. F. Stewart, Acta Crystallogr., Sect. A: Cryst. Phys., Diffr., Theor. Gen. Crystallogr. **33**, 823 (1977).
[76] V. Milman, B. Winkler, J. A. White, C. J. Pickard, M. C. Payne, E. V. Akhmatskaya, and R. H. Nobes, Int. J. Quantum Chem. **77**, 895 (2000).
[77] M. C. Payne, M. P. Teter, D. C. Allan, and J. D. Joannopoulos, Rev. Mod. Phys. **64**, 1045 (1992) and references therein.
[78] J. P. Perdew and A. Zunger, Phys. Rev. B **23**, 5048 (1981).
[79] D. M. Ceperley and B. J. Alder, Phys. Rev. Lett. **45**, 566 (1980).
[80] J. P. Perdew, K. Burke, and M. Ernzerhof, Phys. Rev. Lett. **77**, 3865 (1996).
[81] J. A. White and D. M. Bird, Phys. Rev. B **50**, 4954 (1994).
[82] A. D. Becke, J. Chem. Phys. **84**, 4524 (1986); J. P. Perdew, Phys. Rev. B **33**, 8822 (1986).
[83] J. P. Perdew and Y. Wang, Phys. Rev. B **33**, 8800 (1986).
[84] N. Troullier and J. L. Martins, Phys. Rev. B **43**, 1993 (1991).
[85] L. Kleinman and D. M. Bylander, Phys. Rev. Lett. **48**, 1425 (1982).
[86] D. Vanderbilt, Phys. Rev. B **41**, 7892 (1990).
[87] H. J. Monkhorst and J. D. Pack, Phys. Rev. B **13**, 5188 (1976).
[88] J. S. Lin, A. Qteish, M. C. Payne, and V. Heine, Phys. Rev. B **47**, 4174 (1993).
[89] G. P. Francis and M. C. Payne, J. Phys.: Condens. Matter **2**, 4395 (1990).
[90] J. C. Charlier, X. Gonze, and J. P. Michenaud, Europhys. Lett. **28**, 403 (1994).
[91] J. V. Badding, and T. J. Scheidemantel, Solid State Commun. **122**, 473 (2002).
[92] N. Jacobson, B. Tegner, E. Schröder, P. Hyldgaard, and B. I. Lundqvist, Comput. Mater. Sci. **24**, 273 (2002).
[93] R. Clarke and C. Uher, Adv. Phys. **33**, 469 (1904).
[94] F. D. Murnaghan, Proc. Natl. Acad. Sci. U.S.A. **30**, 244 (1944).
[95] S. S. Kabalkina and L. F. Vereshchagin, Sov. Phys. Dokl. **5**, 373 (1960) [Dokl. Akad. Nauk SSSR **131**, 200 (1960)].
[96] N. Wada, R. Clarke, and S. A. Solin, Solid State Commun. **35**, 675 (1980).
[97] H. Zabel and S. A. Solin, *Graphite Intercalation Compounds* (Springer-Verlag, New York, 1990), Vol. 1.
[98] N. Wada, Phys. Rev. B **24**, 1065 (1981).
[99] M. Maeda, Y. Kuramoto, and C. Horie, J. Phys. Soc. Jpn. **47**, 337 (1979).
[100] M. Grimsditch, J. Phys. C **16**, L143 (1983).
[101] H. Zabel, A. Magerl, and J. J. Rush, Phys. Rev. B **27**, 3930 (1983).
[102] W. A. Kamitakahara, J. Phys. Chem. Solids **6–8**, 671 (1996).
[103] A. P. P. Nicholson and D. J. Bacon, J. Phys. C **10**, 2295 (1977).
[104] G. J. Ackland, Phys. Rev. Lett. **80**, 2233 (1998); **81**, 3301 (1998).